Sliding Mode Observer-Based Robust Switch Fault Diagnosis of Bidirectional Interleaved Converters for Energy Storage System

Shengrong Zhuo, *Member, IEEE*, Yuqi Ma, Ruixin Zhang, Yigeng Huangfu, *Senior Member, IEEE*, and Fei Gao, *Fellow, IEEE*

***Abstract*—Reliable operation of the dc–dc power converter interfaced with the energy storage system is vital for many mission-critical applications, where a reliable fault diagnosis is essential. In this article, a robust switch open-circuit fault diagnosis method based on sliding mode observer is proposed and then applied to a bidirectional interleaved buck/boost converter for the energy storage system. It uses the sliding mode observer to generate the residual, which is then sent to the evaluation module to make the fault decisions. Thanks to the robustness of the sliding mode control algorithm, the generated residual decouples the uncertainties and disturbances with the switch faults. Therefore, it shows strong immunity to the circuit parameter uncertainties and load disturbances. Furthermore, as the diagnosis variables, namely, the inductor currents, are within the closed-loop control system, the extra sensors are not needed. The effectiveness and robustness of the proposed fault diagnosis method have been demonstrated by both the simulation and experimental results.**

***Index Terms*—Bidirectional interleaved converter, dc–dc power converter, fault diagnosis, sliding mode observer, switch open-circuit fault (OCF).**

I. Introduction

DUE to the issues of the energy crisis and environmental pollution, the development of new energy sources, such as photovoltaics, wind turbines, and fuel cells, has been obtaining more and more research attention, especially in the fields of power generation and electrified transportation [1], [2]. To fully exploit these sustainable and intermittent energies, the energy storage device that can emit and absorb the electrical energy, for example, a battery, plays an important role in ensuring the system's stable operation [3]. To address the voltage mismatch between the battery and the dc bus, the bidirectional dc–dc converter is generally interfaced [4]. The dc–dc interleaved buck/boost converter, which features high efficiency, low current stress, and low current ripple, is an attractive choice. In mission-critical and safety-critical applications, the reliability of the power converter is of utmost importance. An industry survey has shown that the power semiconductor device is one of the most fragile components [5]. It accounts for about 30% of malfunctions and breakdowns, mainly including the switch open-circuit fault (OCF) and switch short-circuit fault (SCF). The switch SCF is very serious, and typically, the smart driver or fuse is employed to convert it into OCF. The switch failure can lead to degraded control performance, component overstresses, large current ripple, and even second failure. Therefore, to protect the converter circuit and ensure the continuous operation of the system after the faults, fast and reliable fault diagnosis is essential.

The switch fault diagnosis methods reported in the literature mainly can be classified into three categories: model-based method, signal-based method, and data-based method. The data-based method requires a substantial amount of data to train the diagnostic system utilizing artificial intelligence techniques, including linear regression, support vector machine, and neural networks, among others. In [6], the linear regression-based method is proposed to diagnose the switch fault for dc–dc boost converters in photovoltaic applications. Moreover, the deep neural networks-based diagnosis method is proposed in [7] to further improve the diagnosis accuracy. The comparison results with the support vector machine method validate its superiority. In general, as summarized in [8], the limitations are that the data acquisition and training process is relatively complicated. Therefore, it is preferred for fault diagnosis of large and complex systems. The signal-based method relies on directly sensing signals that carry information about the specific fault and extracting their features as symptoms. Fault diagnosis is achieved by analyzing these symptoms in both the healthy and fault modes. The commonly used signals for dc–dc converters are switch terminal voltage [9], diode terminal voltage [10], output voltage [11], [12] inductor voltage [13], [14], inductor current [15], [16], [17], and input current [18], [19], [20]. For instance, in [11], the magnetic component (inductor or transformer) voltage is sensed by inserting an auxiliary winding, and the switch fault in the

Received 10 October 2024; revised 3 January 2025 and 22 February 2025; accepted 25 February 2025. Date of publication 28 February 2025; date of current version 14 April 2025. This work was supported by the Guangdong Basic and Applied Basic Research Foundation under Grant 2025A1515010436. Recommended for publication by Associate Editor A. Kuperman. *(Corresponding author: Shengrong Zhuo.)*

Shengrong Zhuo is with the Shenzhen Research Institute of Northwestern Polytechnical University, Shenzhen 518057, China (e-mail: srzhuo@nwpu.edu.cn).

Yuqi Ma, Ruixin Zhang, and Yigeng Huangfu are with the School of Automation, Northwestern Polytechnical University, Xi'an 710072, China (e-mail: yuqima@mail.nwpu.edu.cn; rxzhang@mail.nwpu.edu.cn; yigeng@nwpu.edu.cn).

Fei Gao is with the Marie and Louis Pasteur University, UTBM, CNRS, FEMTO-ST Institute, 90010 Belfort, France (e-mail: fei.gao@utbm.fr).

Color versions of one or more figures in this article are available at https://doi.org/10.1109/TPEL.2025.3546570.

Digital Object Identifier 10.1109/TPEL.2025.3546570

power converters can be diagnosed based on the switch ON-OFF signals. The diagnosis speed is very fast, while it needs extra hardware sensors/circuitry, which is invasive. Alternatively, in [15], the inductor current slope and the gate driver signal are exploited to diagnose the switch fault for boost converters. The extra sensors are not needed, as the inductor current is already within the closed-loop control system. However, it requires an extremely high sampling frequency to obtain the slope signal and it is limited to the specific converters.

Model-based methods have recently become increasingly attractive, with the significant advancement of digital signal processors. This method was originally developed to substitute hardware redundancy with analytical redundancy [21]. To be specific, it involves generating and evaluating the residual, which is defined as the difference between the measured output of the actual converter and the predicted output from the converter mathematical model. As the converter model is generally available, it allows the extension to any power converters. However, one limitation is that it requires a precise converter model to ensure an accurate diagnosis. For example, in [22], a switching model-based state estimator approach is designed for fault detection and identification for various types of power converters. Since the residual is generated through open-loop state estimation, this diagnosis method exhibits poor robustness to model imperfections. Consequently, an accurate converter model is necessary to minimize false alarms. However, in practical applications, it is not realistic to acquire the precise converter model without errors, as the converter circuit parameter may deviate due to manufacturing and aging. To this end, the state-space observer with residual feedback is devised in [23] for interleaved buck converters. Moreover, the immersion and invariant observer and the Luenberger observer with residual feedback are developed respectively in [24], [25], and [26] for interleaved boost converters. Thanks to the introduced residual feedback, the robustness of the diagnosis method to the modeling errors is allowed.

The above diagnosis methodologies are primarily designed for unidirectional converters. The bidirectional dc–dc power converter for energy storage systems has different operating modes (buck mode, boost mode, and critical mode), its switch fault diagnosis cannot be solved effectively by directly applying the previous methods. If the fault diagnosis methods in [23], [24], [25], and [26] are used for the bidirectional dc–dc converters, multiple state observers are required to conduct the complete diagnosis of switch faults. This would reduce the diagnosis efficiency and increase the diagnosis workload at the same time. Therefore, in [27] and [28], a global state observer-based method is proposed to diagnose the switch fault for the bidirectional buck/boost converters in a hybrid energy source system. It uses only one state observer to generate the residual. However, since the state observer used is a linear observer, the decoupling of the generated residual for the switch fault and the modeling uncertainties is incomplete. As shown later, it does not solve the impact of the deviation of electronic component parameters, thus influencing the robustness of fault diagnosis.

The sliding mode algorithm has strong immunity against the circuit parameter uncertainties and disturbances [29]. Thus, it has been increasingly used for observer-based fault diagnosis in the fields of motor inter-turn faults [30], inverter faults [31], drive sensor faults [32], and so on. In this article, we propose a robust method for diagnosing switch OCFs based on a sliding mode observer and then apply it to the bidirectional interleaved dc–dc buck/boost converters for energy storage systems. The sliding mode observer is designed to generate residuals for fault diagnosis using only the nominal converter model. It is demonstrated that the proposed method shows strong robustness to modeling imperfections and disturbances. Furthermore, it utilizes the inductor current as the diagnostic variable, which is already within the closed-loop control system. Therefore, no additional sensors are required. The proposed method can be extended to other bidirectional power converters. The main contributions can be summarized as follows.

1) A robust switch fault diagnosis method based on sliding mode observer is proposed and elaborated. It shows great prospects as it only needs the crude converter model with nominal parameters, without using a precise converter model. Moreover, it has strong robustness against the circuit parameter uncertainties and disturbances.
2) The proposed diagnosis method is then applied to the dc–dc interleaved bidirectional buck/boost converters. It does not require additional sensors. The validity of the proposed method is verified by both the simulation and experimental results. It is shown that the switch OCFs can be diagnosed in less than two switching periods.

The rest of the article is organized as follows. In Section II, the description of the energy storage systems and modeling of the bidirectional converter are presented. In Section III, the proposed diagnosis method is elaborated. The simulation and experimental results are provided in Sections IV and V, respectively. Finally, Section VI concludes this article.

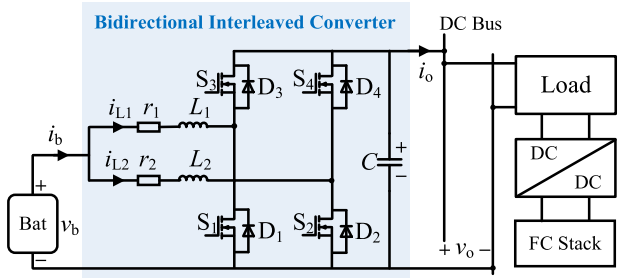

Fig. 1. Structure of the hybrid energy storage system.

II. System Description and Converter Modeling

A. System Description

Fig. 1 illustrates the structure of a hybrid energy storage system, with FC as the primary power source, and battery as the energy buffer to compensate for the power difference between the load and FC stack. For the FC converter, the task is to track the current reference generated by the energy management system. The related controller design can be referred to [33]. Meantime, to stabilize the dc bus to satisfy the load requirement, the bidirectional interleaved buck/boost dc–dc converter is interfaced with the battery. This converter is formed by

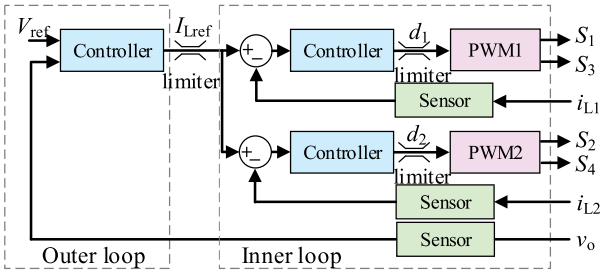

Fig. 2. Dual-loop closed control scheme for bidirectional converter.

associating two buck/boost converter modules with an input-parallel output-parallel structure. For each buck-boost converter module, there is one inductor $L_k(k = 1, 2)$, one equivalent circuit parasitic resistance $r_k(k = 1, 2)$, two power switches S_k, S_{k+2} $(k = 1, 2)$, and two power diodes $\mathrm{D}_k, \mathrm{D}_{k+2}$ $(k = 1, 2)$. C is the bus capacitor.

The primary objective of the bidirectional interleaved dc–dc converter is to regulate the bus voltage while ensuring that power is balanced between the two modules. This helps prevent overloading one of the modules during heavy load conditions. In addition, interleaved techniques that phase shift properly the switching signals can minimize input/output ripple provided that the switching frequency is constant. To achieve these three goals, namely, constant bus voltage, power balancing between modules, and constant switching frequency, a closed-loop control scheme as illustrated in Fig. 2 is commonly used.

It is seen from Fig. 2 that the outer-loop controller produces the reference current for the inner loops to generate the duty cycles, which are limited to [0, 1]. The duty cycles are then sent to the pulsewidth modulation module to acquire the ON-OFF signals for power switches. It should be pointed out that the switch signals for power switches [S_k, S_{k+2} $(k = 1, 2)$] are complementary to prevent any shoot-through.

B. Converter Modeling

The bidirectional converter operates in boost mode when the battery is discharging and in buck mode when the battery is charging. When it works in boost mode, the converter can be modeled as follows, according to Kirchhoff's voltage law

$$\begin{cases} \dfrac{d}{dt} i_{L1} = \dfrac{v_b}{L_1} - \dfrac{r_1}{L_1} i_{L1} - \dfrac{(1-d_1)}{L_1} v_o \\ \dfrac{d}{dt} i_{L2} = \dfrac{v_b}{L_2} - \dfrac{r_2}{L_2} i_{L2} - \dfrac{(1-d_2)}{L_2} v_o \end{cases} \tag{1}$$

where $i_{Lk}(k = 1, 2)$ is the current flowing through the inductor L_k, v_o is the bus voltage, v_b is the battery voltage, $d_k(k = 1, 2)$ is the duty cycle for the switch S_k.

When the converter works in buck mode, the converter model can be expressed as

$$\begin{cases} \dfrac{d}{dt} i_{L1} = \dfrac{v_\mathrm{b}}{L_1} - \dfrac{r_1}{L_1} i_{L1} - \dfrac{d_3}{L_1} v_\mathrm{o} \\ \dfrac{d}{dt} i_{L2} = \dfrac{v_\mathrm{b}}{L_2} - \dfrac{r_2}{L_2} i_{L2} - \dfrac{d_4}{L_2} v_\mathrm{o} \end{cases} \tag{2}$$

where $d_k(k = 3, 4)$ is the duty cycle for the switch S_k.

TABLE I
CONVERTER STATE WITH $\boldsymbol{f}_n(t)$

n	Converter state	$\boldsymbol{f}_n(t)$
0	No fault	$\begin{bmatrix} -\frac{(r_1-r)x_1}{L} \\ -\frac{(r_2-r)x_2}{L} \end{bmatrix}$
1	S_1 OCF	$\begin{bmatrix} -\frac{v_\mathrm{b}-rx_1}{L} \\ -\frac{(r_2-r)x_2}{L} \end{bmatrix}$
2	S_2 OCF	$\begin{bmatrix} -\frac{(r_1-r)x_1}{L} \\ -\frac{v_\mathrm{b}-rx_2}{L} \end{bmatrix}$
3	S_3 OCF	$\begin{bmatrix} -\frac{v_\mathrm{b}-rx_1-v_\mathrm{o}}{L} \\ -\frac{(r_2-r)x_1}{L} \end{bmatrix}$
4	S_4 OCF	$\begin{bmatrix} -\frac{(r_1-r)x_1}{L} \\ -\frac{v_\mathrm{b}-rx_2-v_\mathrm{o}}{L} \end{bmatrix}$

It is noted that due to the complementary switch signals for the power switch of the same branch/module, there exists:

$$d_k = 1 - d_{k+2}, k = 1, 2. \tag{3}$$

Therefore, it follows from (1), (2), and (3) that the converter model in both boost mode and buck mode can be merged into one unified model as follows:

$$\begin{cases} \dot{\boldsymbol{x}}(t) = \underbrace{\begin{bmatrix} \frac{-r_1}{L_1} & 0 \\ 0 & \frac{-r_2}{L_2} \end{bmatrix}}_{\boldsymbol{A}} \boldsymbol{x}(t) + \underbrace{\begin{bmatrix} \frac{1}{L_1} & \frac{d_1-1}{L_1} \\ \frac{1}{L_2} & \frac{d_2-1}{L_2} \end{bmatrix}}_{\boldsymbol{B}} \boldsymbol{u}(t) \\ \boldsymbol{y}(t) = \underbrace{\begin{bmatrix} 1 & 0 \\ 0 & 1 \end{bmatrix}}_{\boldsymbol{C}} \boldsymbol{x}(t) \end{cases} \tag{4}$$

where $\boldsymbol{x}(t) = [x_1, x_2]^T = [I_{L1}, I_{L2}]^T$, $\boldsymbol{u}(t) = [v_b, v_o]^T$.

In general, it is not feasible to acquire the exact circuit parameters of a practical converter. Thus, rewrite the converter model using the nominal parameters, there is

$$\begin{cases} \dot{\boldsymbol{x}}(t) = \boldsymbol{A}_0 \boldsymbol{x}(t) + \boldsymbol{B}_0 \boldsymbol{u}(t) + \boldsymbol{f}_0(t) \\ \boldsymbol{f}_0(t) = (\boldsymbol{A} - \boldsymbol{A}_0) \boldsymbol{x}(t) + (\boldsymbol{B} - \boldsymbol{B}_0) \boldsymbol{u}(t) \\ \boldsymbol{y}(t) = \boldsymbol{C}\boldsymbol{x}(t) \end{cases} \tag{5}$$

$$\boldsymbol{A}_0 = \begin{bmatrix} \frac{-r}{L} & 0 \\ 0 & \frac{-r}{L} \end{bmatrix}, \ \boldsymbol{B}_0 = \begin{bmatrix} \frac{1}{L} & \frac{d_1-1}{L} \\ \frac{1}{L} & \frac{d_2-1}{L} \end{bmatrix} \tag{6}$$

where L and r are, respectively, the nominal inductance and lumped resistance of the converter circuit.

Furthermore, consider the case of OCF in switch $\mathrm{S}_n(n = 1, 2, 3, 4)$, define the deviation of matrix $\boldsymbol{A}$ and $\boldsymbol{B}$ as $\Delta\boldsymbol{A}$ and $\Delta\boldsymbol{B}$, respectively, and the converter model becomes

$$\begin{cases} \dot{\boldsymbol{x}}(t) = \boldsymbol{A}_0 \boldsymbol{x}(t) + \boldsymbol{B}_0 \boldsymbol{u}(t) + \boldsymbol{f}_n(t) \\ \boldsymbol{f}_n(t) = \boldsymbol{f}_0(t) + \Delta\boldsymbol{A}\boldsymbol{x}(t) + \Delta\boldsymbol{B}\boldsymbol{u}(t) \\ \boldsymbol{y}(t) = \boldsymbol{C}\boldsymbol{x}(t) \end{cases} \tag{7}$$

where $n \in \{1, 2, 3, 4\}$ represents the fault location of S_n.

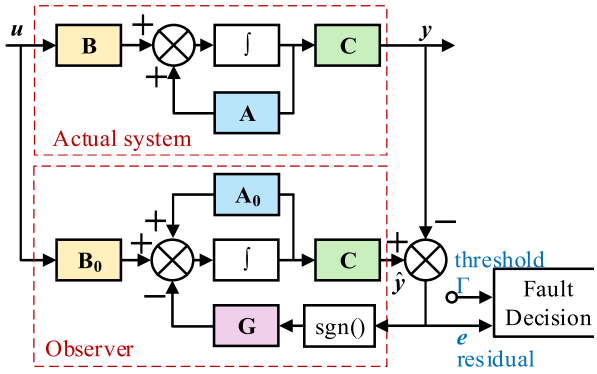

Fig. 3. Scheme of the proposed diagnosis method based on sliding mode observer.

Table I summarizes the relationship between n, converter health state, and corresponding $\boldsymbol{f}_n(t)$. It should be pointed out that the $n = 0$ represents the healthy converter with no fault.

III. Proposed Fault Diagnosis Method

A. Fault Diagnosis Scheme

The kernel of the model-based fault diagnosis method is to analyze the difference between the measured characteristic variable from the actual system and its estimated value by the system model. This difference is termed as the residual. The process of model-based fault diagnosis can be divided into two steps: residual generation, and residual evaluation. In this article, the inductor currents are selected as the characteristic variable to diagnose the switch fault. This is mainly because it has existed in the closed-loop controller, and no additional sensors are required. Moreover, to explore the robustness of the sliding mode algorithm to the uncertainties and disturbances [33], the sliding mode observer is used to generate the residual. After evaluating the residuals, the switch fault can be diagnosed.

Fig. 3 shows the fault diagnosis scheme based on the sliding mode observer. The observer is construed to generate the residuals, based on the nominal converter model in the health state, as established in (5). It shares the same input as the actual converter system. In particular, the residual feedback is used to compensate for the modeling imperfections caused by the uncertain circuit parameters. Finally, the residuals are evaluated by comparing them with the threshold to make fault decisions.

B. Residual Generation Based on Sliding Mode Observer

The sliding mode observer is designed as follows to estimate the inductor currents, based on the nominal model in (5)

$$\begin{cases} \dot{\hat{\boldsymbol{x}}}(t) = \boldsymbol{A}_0\,\hat{\boldsymbol{x}}(t) + \boldsymbol{B}_0\boldsymbol{u}(t) - \underbrace{\begin{bmatrix} g_1 & 0 \\ 0 & g_2 \end{bmatrix}}_{\boldsymbol{G}} \operatorname{sgn}(\boldsymbol{e}(t)) \\ \hat{\boldsymbol{y}}(t) = \boldsymbol{C}\hat{\boldsymbol{x}}(t) \end{cases} \tag{8}$$

where $\hat{\boldsymbol{x}}(t)$ and $\hat{\boldsymbol{y}}(t)$ are the estimated variables for $\boldsymbol{x}(t)$ and $\boldsymbol{y}(t)$, respectively. $\boldsymbol{e}(t) = \hat{\boldsymbol{y}}(t) - \boldsymbol{y}(t)$ is the residual, and $\operatorname{sgn}(\cdot)$ is a standard sign function. g_1 and g_2 are observer gains to be tuned, and there are: $g_1 > 0$, $g_2 > 0$.

The stability of the above observer can be analyzed using the Lyapunov theory, see Appendix A.

C. Residual Evaluation Under Switch Fault

It follows from (5), (7), and (8) that the residual generated by the sliding mode observer can be expressed as

$$\dot{\boldsymbol{e}}(t) = \boldsymbol{A}_0\,\boldsymbol{e}(t) - \boldsymbol{G}\operatorname{sgn}(\boldsymbol{e}(t)) - \boldsymbol{f}_n(t), n = 0,1,2,3,4. \tag{9}$$

It is obvious from (6) that $\boldsymbol{A}_0 < 0$. Therefore, the time evolution of the residual $\boldsymbol{e}(t)$ becomes

$$\boldsymbol{e}(t) = -\left(\boldsymbol{G}\operatorname{sgn}(\boldsymbol{e}(t)) + \boldsymbol{f}_n(t)\right)\int_0^t e^{\boldsymbol{A}_0(t-\tau)}d\tau. \tag{10}$$

To exploit the residual to deliver the fault message, it is expected that the residual maintains at zero in converter healthy mode, while diverging considerably in switch fault mode. To achieve this goal, the observer gains should satisfy

$$|\boldsymbol{f}_0(k)| \le g_k \le |\boldsymbol{f}_n(k)|, k = 1,2; n = 1,2,3,4. \tag{11}$$

The converter trajectories are bounded, as proved in Appendix B. The bidirectional converter can operate in either discharging mode or charging mode. The discharging tube and the charging tube cannot operate simultaneously. Thus, the fault diagnosis of the discharging and charging tubes can be discussed as follows.

1) Discharging Tubes S_1 and S_2: In converter healthy mode, it follows from (10) and (11) that the residuals become

$$\boldsymbol{e} = \begin{bmatrix} e_1 \\ e_2 \end{bmatrix} = \begin{bmatrix} 0 \\ 0 \end{bmatrix}. \tag{12}$$

Without loss of generality, assume that the OCF occurs in power switch S_1. It is derived from (10) and (11) that the residual vector is

$$\boldsymbol{e} = \begin{bmatrix} e_1 \\ e_2 \end{bmatrix} = \begin{bmatrix} \frac{v_b - rx_1 - g_1 L}{r} \\ 0 \end{bmatrix}. \tag{13}$$

Similarly, suppose that the OCF takes place in switch S_2, the residual vector changes to

$$\boldsymbol{e} = \begin{bmatrix} e_1 \\ e_2 \end{bmatrix} = \begin{bmatrix} 0 \\ \frac{v_b - rx_2 - g_2 L}{r} \end{bmatrix}. \tag{14}$$

Therefore, it can be concluded that the failure in switch $\mathrm{S}_k (k = 1,2)$ only influences its corresponding residual. The related residual is zero in healthy mode, and it becomes a positive value of $\frac{v_b - rx_k - g_k L}{r}$ in switch fault mode.

2) Charging Tubes S_3 and S_4: In converter healthy mode, the residuals are the same as that in (12). Consider the switch OCF in switch S_3, according to (10) and (11), the residuals turn into

$$\boldsymbol{e} = \begin{bmatrix} e_1 \\ e_2 \end{bmatrix} = \begin{bmatrix} \frac{v_b - rx_1 - v_o + g_1 L}{r} \\ 0 \end{bmatrix}. \tag{15}$$

When switch OCF happens in switch S_4, the residuals are as follows:

$$\boldsymbol{e} = \begin{bmatrix} e_1 \\ e_2 \end{bmatrix} = \begin{bmatrix} 0 \\ \frac{v_b - r x_2 - v_o + g_2 L}{r} \end{bmatrix}. \tag{16}$$

Similarly, the influence of the switch fault on its residual is independent. When OCF occurs in the switch $\mathrm{S}_{k+2}(k = 1, 2)$, the residual changes from zero to a negative value $\frac{v_b - r x_k - v_o + g_k L}{r}$.

D. Fault Diagnosis and Fault Decision

According to the above residual evaluation in Section III-C, it is seen that in the converter healthy mode, the residual vector is zero. When the converter operates in discharging mode, i.e., the battery current $i_b > 0$, the related residual would diverge to a positive value if switch OCF occurs in discharging tubes S_1 and S_2. Similarly, when the converter works in charging mode, i.e., the battery current $i_b < 0$, the related residual would change to a negative value if switch OCF happens in charging tubes S_3 and S_4. The battery current can be calculated by $i_b = i_{L1} + i_{L2}$, according to the topology in Fig. 1. Therefore, the switch OCFs can be diagnosed based on the following logic:

$$\mathrm{Flag}_1 = \begin{cases} 1 \; i_b > 0 \text{ and } e_1 > \Gamma_1 \\ 0 \text{ otherwise} \end{cases} \tag{17}$$

$$\mathrm{Flag}_2 = \begin{cases} 1 \; i_b > 0 \text{ and } e_2 > \Gamma_2 \\ 0 \text{ otherwise} \end{cases} \tag{18}$$

$$\mathrm{Flag}_3 = \begin{cases} 1 \; i_b < 0 \text{ and } e_1 < -\Gamma_1 \\ 0 \text{ otherwise} \end{cases} \tag{19}$$

$$\mathrm{Flag}_4 = \begin{cases} 1 \; i_\mathrm{b} < 0 \text{ and } e_2 < -\Gamma_2 \\ 0 \text{ otherwise} \end{cases} \tag{20}$$

where Flag_1, Flag_2, Flag_3, and Flag_4 are, respectively, the switch OCF flags for the power switch S_1, S_2, S_3, and S_4. When the flag equals one, it is indicated that there is a switch OCF. Γ_k is the diagnosis threshold to be set, which satisfy:

$$0 < \Gamma_k < \min\left(\left| \frac{v_b - r x_k - g_k L}{r} \right|, \left| \frac{v_b - r x_k - v_C + g_k L}{r} \right| \right), \quad k = 1, 2. \tag{21}$$

IV. Simulation Validation

To demonstrate the validity of the proposed method, both the energy storage system shown in Fig. 1 and the proposed fault diagnosis method are implemented based on the software MATLAB/Simulink. The main circuit parameters of the bidirectional interleaved dc–dc buck/boost converter are given in Table II. The non-ideal power switches and diodes with default circuit parameters are used. The inductance is 800 μH, the equivalent series resistance of the inductor is 0.6 Ω, and the capacitance is 1000 μF. The switching frequency is 25 kHz, the inductor is sampled twice in one switching cycle to obtain its average value. The sampling frequency for the voltages is equal to the switching frequency. Substitute the limit value of the inductor current and consider the parasitic resistance deviation by 50%, the observer gains can be set as $g_1 = g_2 = 2500$ based on (11). The threshold value should satisfy (21), and it is tuned as $\Gamma_1 = \Gamma_2 = 0.4$ by balancing the accuracy and rapidity of the switch fault diagnosis.

TABLE II
Circuit Parameters of the Bidirectional Converter

Description	Variable	Value
Inductor	L_1, L_2	800 μH
Inductor resistance	r_1, r_2	0.6 Ω
Capacitor	C	1000 μF
Output bus voltage	V_{ref}	48 V
Battery voltage	V_b	22.4 V
Inductor current	$I_{\mathrm{L1}}, I_{\mathrm{L2}}$	0 ~ ±6 A
Switching frequency	f_s	25 kHz

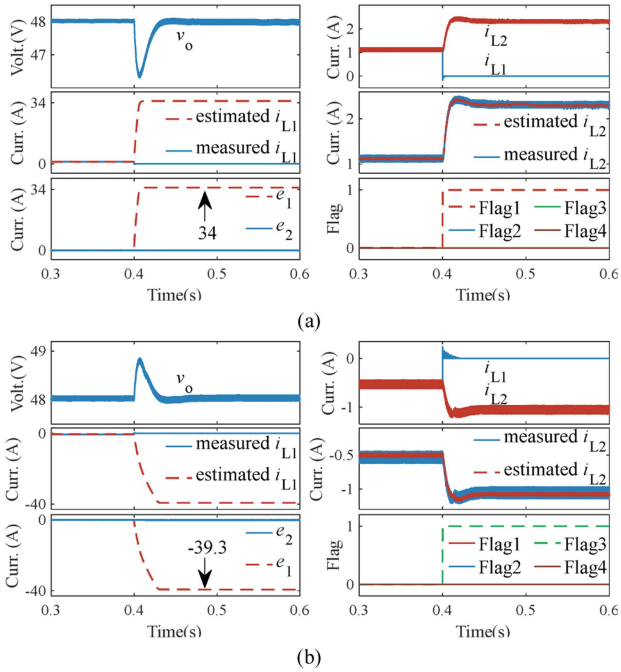

Fig. 4. Fault diagnosis for single switch OCF. (a) OCF occurs in switch S_1 at $t = 0.4$ s. (b) OCF happens in switch S_3 at $t = 0.4$ s.

A. Diagnosis of Switch OCF

For the energy storage system, set the FC voltage as 25 V, and its current as 2 A. Meantime, set the load current as 2 A. Since the reference bus voltage is 48 V, at this time, the battery works in discharging mode to supply the power to the load to stabilize the dc bus. It is seen from Fig. 4(a) that at the start, the converter works in healthy mode, the output voltage can be regulated at the desired value of 48 V, and the current balancing between the two converter modules is achieved. It is also noted that the estimated current can accurately track the measured current. Thus, the resulting residuals e_1 and e_2 are located in the vicinity of zero, and the flags are equal to zero, implying the healthy state of the converter.

Without loss of generality, applying the OCF to switch S_1 at $t = 0.4$ s. It is observed from Fig. 4(a) that the inductor current

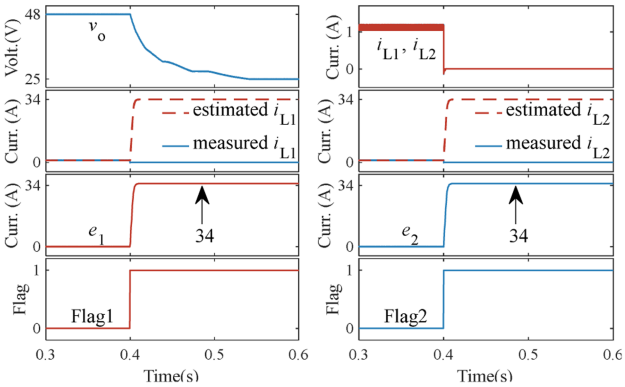

Fig. 5. Fault diagnosis for double switch OCFs in S_1 and S_2.

i_{L1} in the faulty module decreases to zero soon, and the inductor current i_{L2} in the rest healthy module increases to stabilize again the dc bus. It is also shown that the estimated value $\hat{i}_{L1}$ for the inductor current i_{L1} in faulty module diverges. The relevant residual e_1 exceeds the threshold quickly, and triggers the flag signal. It finally arrives at the value of 34, which is consistent with the calculated value by (13). The OCF in switch S_1 is thus diagnosed. Moreover, it is noticed that the other estimated value $\hat{i}_{L2}$ can still follow the inductor current i_{L2} in the healthy module. The related residual e_2 is always under the threshold, without generating a false alarm.

Furthermore, change the load current to 0.5 A. In this case, the battery works in charging mode to absorb the excessive power from the load side. It is noticed in Fig. 4(b) that at the beginning, the converter operates in a healthy mode, and the output voltage is equal to the reference value of 48 V. The sliding mode observer functions well to track the inductor currents and the residuals e_1 and e_2 are very close to zero. Therefore, the flags are equal to zero, indicating the healthy state of the converter.

Applying the OCF to switch S_3 at $t = 0.4$ s. It is noted from Fig. 4(b) that the inductor current i_{L1} in the faulty module rises to zero promptly, and the rest inductor current i_{L2} drops to compensate for the lost module. Moreover, as the estimated value $\hat{i}_{L1}$ diverges, the relevant residual e_1 goes over the threshold, and activates the flag signals rapidly to identify the OCF in switch S_3. The threshold finally arrives at the value of –39.3, which agrees with the calculated value by (15). In contrast, the other estimated value $\hat{i}_{L2}$ can still track the inductor current i_{L2} in the healthy module. The relevant residual e_2 is always below the threshold, there is no false alarm.

As analyzed in Section III-C, the influence of the switch fault on its residual is independent. Therefore, the proposed method can diagnose simultaneously the multiple power switches. Take the converter discharging mode as an example, the simulation results are plotted in Fig. 5. It is seen that at the beginning, the converter operates in healthy mode, the bus voltage is regulated at the reference value, and the residuals are under the threshold, the flag signals are zero. However, when applying the OCFs to both switch S_1 and S_2 $t = 0.4$ s, it is noted that the two inductor currents decay to zero rapidly, and the bus voltage cannot be maintained anymore. Meanwhile, the two residuals e_1 and e_2 surpass the threshold quickly, and trigger the flag signals to identify the switch faults. Both the residuals reach the value of 34, which is in line with the calculated values by (13) and (14). The effectiveness and correctness of the theoretical analysis in Section III-C are verified.

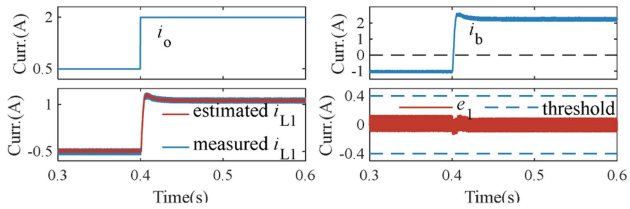

Fig. 6. Simulation results of the power converter in healthy mode under disturbances.

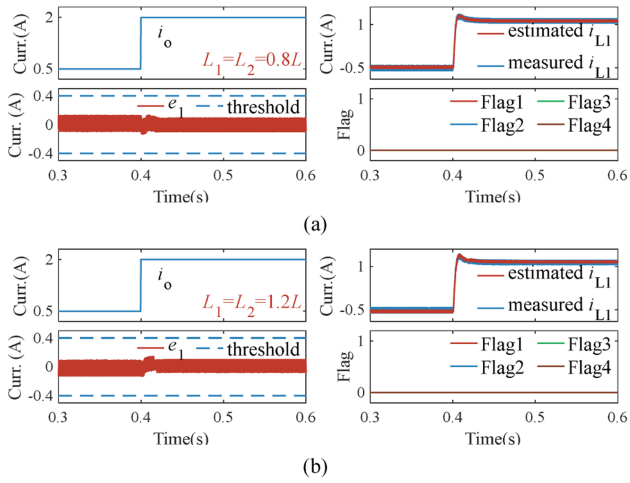

Fig. 7. Simulation results of the converter in healthy mode under inductance deviation. (a) $L_1 = L_2 = 640\,\mu$H. (b) $L_1 = L_2 = 960\,\mu$H.

B. Robustness to Disturbances and Uncertainties

The proposed diagnosis method features strong robustness to the unknown disturbances and converter uncertainties. Fig. 6 presents the converter in healthy mode under disturbances. It is seen that at the start, the load current is 0.5 A, and the converter operates in charging mode. The residual is always under the threshold, without triggering false alarms. The load current disturbance stepping from 0.5 to 2 A is applied to the system at $t = 0.4$ s, and it is observed that the converter turns to discharge mode, while the residual is still under the threshold, without false alarms. The robustness of the proposed fault diagnosis method to the load disturbance is thus validated.

The proposed diagnosis method is also robust against the converter circuit parameter uncertainties. The converter model only relates to the inductance and the parasitic resistance, see (4) and (5). Fig. 7 plots the simulation results of the converter in healthy mode under inductance deviations by ±20%. The load current stepping from 0.5 to 2 A is applied to the system at $t = 0.4$ s. The converter changes from the charging mode to the discharging mode. It is noted from the figure that the estimated

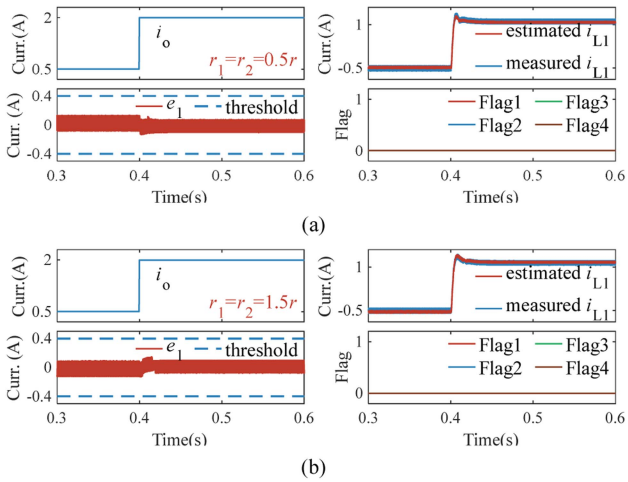

Fig. 8. Simulation results of the converter in healthy mode under parasitic resistance deviation. (a) $r_1 = r_2 = 0.3\,\Omega$. (b) $r_1 = r_2 = 0.9\,\Omega$.

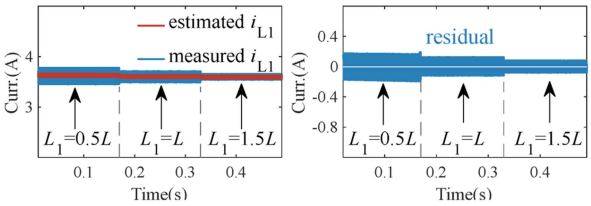

Fig. 9. Simulation results of the power converter under inductance deviation from -50% to 50%.

value can well follow the inductor current, and the residual is always below the threshold. Therefore, the flag signals are not activated, without false alarms.

Fig. 8 shows the simulation results of the converter in healthy mode under parasitic resistance deviation by $\pm 50\%$. At $t = 0.4$ s, the load current steps to 2 A, and the converter operates from discharging to charging mode. It is noticed that the inductor current can be observed well, and the residuals are less than the threshold value. The flags are not triggered, identifying the healthy state of the converter.

C. Discussion

The proposed diagnosis method is independent of the battery voltage v_b. This is because, in practical applications, there is $v_b \gg r_n x_n (n = 1, 2)$, as otherwise, the converter efficiency would be too low. Thus, the distinction between the case of "no fault" and "switch OCF" in Table I is very obvious. Meantime, the diagnosis threshold would not be too small.

Moreover, as shown in (10), the residual has no direct connection with the inductance value of the converter prototype. Fig. 9 shows the simulation results with more severe inductance deviation. It is noticed that the average value of the residual maintains at zero, validating the robustness to the inductance deviation. In addition, it follows from (11) that it is feasible to increase the observer gain to tolerate larger parasitic resistance deviation. It is calculated by (11) that with the observer gain of

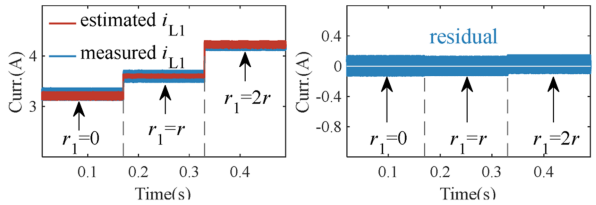

Fig. 10. Simulation results of the power converter under parasitic resistance deviation from -100% to 100%, observer gain $g_1 = g_2 = 5000$.

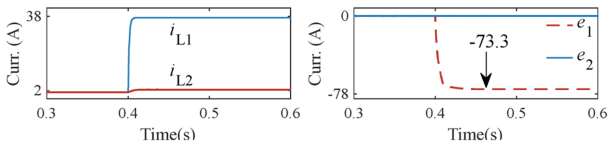

Fig. 11. Simulation results of the power converter under switch S_1 SCF at $t = 0.4$ s.

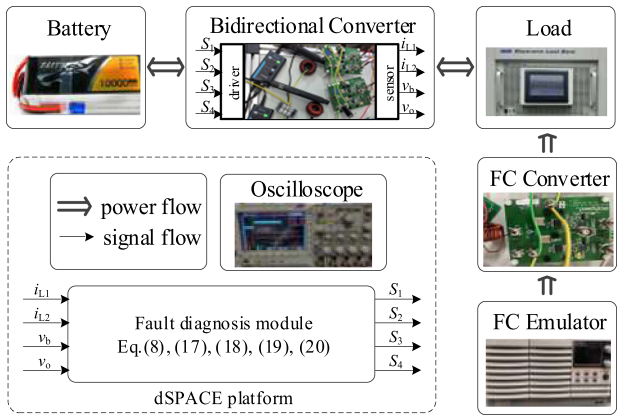

Fig. 12. Experimental rig.

$g_1 = g_2 = 5000$, it is allowed to tolerate the parasitic resistance deviation up to $\pm 100\%$, see Fig. 10.

Finally, the proposed diagnosis method is designed to detect and diagnose the switch OCFs. Fig. 11 shows the case of SCF in switch S_1, it is seen that the residual is less than the lower boundary of the threshold. It follows from (17) that this would not trigger the switch OCF alarm, validating the robustness of the proposed diagnosis method.

V. Experimental Results

To further validate the effectiveness and robustness of the proposed diagnosis method, the converter prototype has been built, with the same circuit parameters given in Table II. The nominal inductance is 800 μH, and the inductor resistance is 0.6 Ω. The nominal capacitance is 1000 μF, and the switching frequency is 25 kHz. The power switch with the reverse diode of C3M0060065J is used. The nominal voltage of the battery is 22.4 V. The diagnosis method with the same observer gains and thresholds is implemented into the dSPACE platform. Fig. 12 shows the experimental rig.

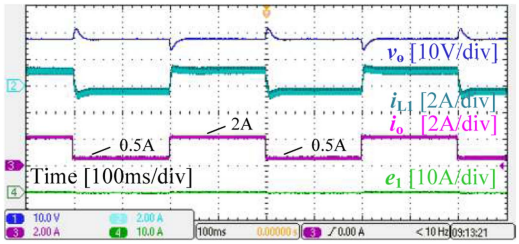

Fig. 13. Experimental results of the power converter in healthy mode under load step disturbances.

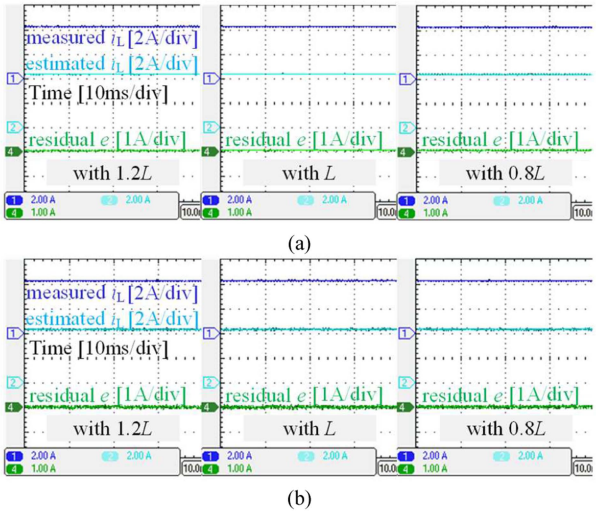

Fig. 14. Experimental results of the power converter in healthy mode under inductance deviation. (a) Linear observer method. (b) Proposed one.

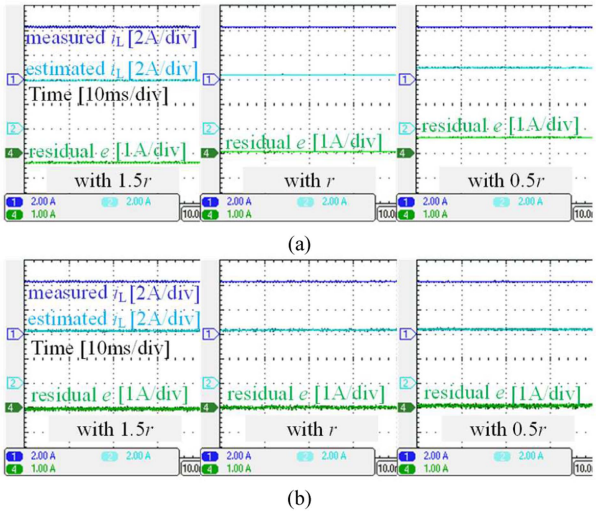

Fig. 15. Experimental results of the power converter in healthy mode under parasitic resistance deviation. (a) Linear observer method. (b) Proposed one.

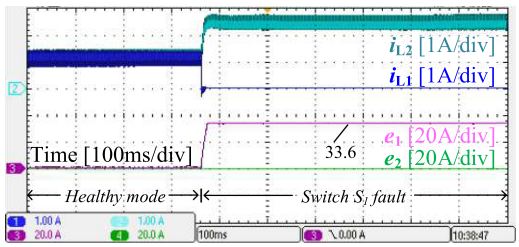

Fig. 16. Experimental results of the converter under OCF in switch S_1.

A. Immunity to Disturbances and Uncertainties

Fig. 13 shows the experimental results of the bidirectional converter in healthy mode under load disturbances. The obtained results are similar to the simulation results in Fig. 6. The load current stepping from 0.5 to 2 A and then backing to 0.5 A is applied to the system periodically. With the closed-loop voltage control, the bus voltage can be maintained at the reference value of 48 V, and the battery changes between the charging and discharging modes. It is observed from the figure that the residual e_1 is always within the vicinity of zero. The residual e_2, which is not shown, has a similar performance. The immunity of the proposed diagnosis method to the load disturbances is thus demonstrated.

Fig. 14 displays the experimental results of the bidirectional converter in healthy mode under inductance deviation. It is not very convenient to change the inductance in the converter prototype at will, therefore, the deviation is implemented by altering the circuit parameter of the converter model by $\pm 20\%$. It is seen from Fig. 14(a) and (b) that no matter with the linear observer method in [26] or the proposed one, the estimated inductor current can well track the measured value, and the residual is very small near zero. The robustness of the two diagnosis methods to the inductance deviation is validated.

Fig. 15 presents the experimental results of the bidirectional converter in healthy mode under parasitic resistance deviation by $\pm 50\%$, which is carried out by varying the circuit parameters in the converter model. It is observed from Fig. 15(a) that with the liner observer method, there exist obvious estimation errors, resulting in considerable residual exceeding the threshold to generate false alarms. In contrast, for the proposed diagnosis method of Fig. 15(b), the residual is always near zero. The stronger robustness of the proposed diagnosis method against the parasitic resistance deviation is verified.

B. Diagnosis of Switch Fault

As analyzed in Section III-C, the power switches in the bidirectional converter can be classified into two categories. The first category is the discharging tubes S_1 and S_2, and the second category is the charging tubes S_3 and S_4.

First, set the load current as 2 A. Since the FC voltage is 25 V, and its current is 2 A, the battery works in discharging mode to compensate for the power mismatch between the load and FC stack. Fig. 16 shows the experimental results of the converter under OCF in switch S_1, which are similar to the simulation results in Fig. 4(a). It is observed that in the beginning, the converter operates in healthy mode, and the residuals are near zero. However, when the OCF occurs in S_1, the inductor current of the faulty module reduces to zero, while the current in the healthy

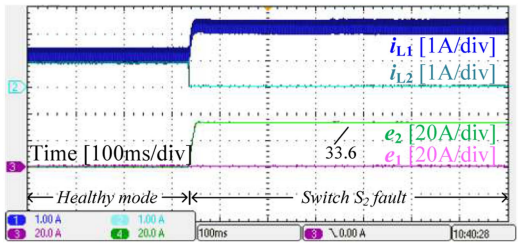

Fig. 17. Experimental results of the converter under OCF in switch S_2.

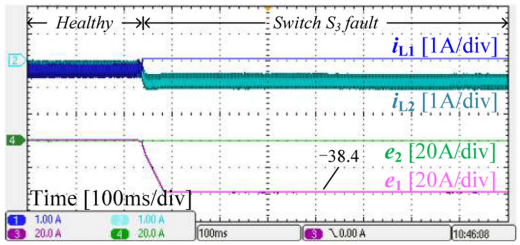

Fig. 18. Experimental results of the converter under OCF in switch S_3.

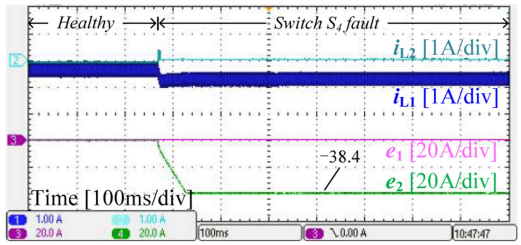

Fig. 19. Experimental results of the converter under OCF in switch S_4.

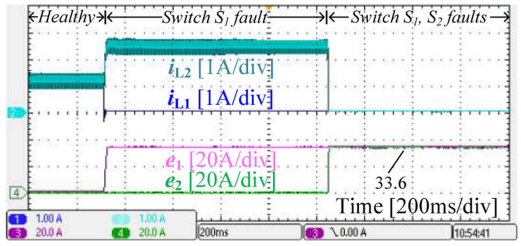

Fig. 20. Experimental results of the converter under OCFs in both switch S_1 and S_2.

module increases to compensate for the lost one. Meantime, it is noted from the figure that the residual e_2 still maintains near the zero. However, the residual e_1 increases quickly, and it exceeds the pre-set threshold in a short time. The OCF in switch S_1 can be diagnosed accurately.

Similarly, the experimental results of the converter under OCF in switch S_2 are plotted in Fig. 17. It is seen that when the switch OCF happens in switch S_2, the inductor current for the faulty module drops to zero, and the rest healthy module rises to achieve continuous operation. It is noticed that the residual e_1 for the healthy phase is always near zero, while the residual e_2 for the faulty phase increases quickly, and it goes over the threshold quickly. The OCF in switch S_2 is thus diagnosed.

Second, set the load current as 0.5 A. Since the FC voltage is 25 V, and its current is 2 A, the battery works in charging mode to absorb the excessive power. Fig. 18 shows the experimental results of the converter under OCF in switch S_3, which is similar to the simulation results in Fig. 4(b). It is observed that in the beginning, the converter operates in healthy mode, and the residuals are near zero. However, when the OCF occurs in S_3, the inductor current of the faulty phase increases to zero, while the current in the healthy phase decreases. Meantime, it is noted from the figure that the residual e_2 still maintains near the zero. However, the residual e_1 decreases rapidly, and it goes over the threshold. The OCF in switch S_3 is diagnosed.

Similarly, the experimental results of the converter under OCF in switch S_4 are presented in Fig. 19. It is noted that when the switch OCF takes place in switch S_4, the inductor current for the faulty module rises to zero, and the rest healthy phase drops. Moreover, the residual e_1 for the healthy module is always near zero, while the residual e_2 for the faulty module decreases, and it surpasses the threshold quickly. The OCF in switch S_4 is diagnosed.

TABLE III
STEADY-STATE RESIDUAL VALUE IN THE FAULTY MODULE

Case	Experimental observation	Theoretical calculation
S_1 OCF	33.6	34
S_2 OCF	33.6	34
S_3 OCF	–38.4	–39.3
S_4 OCF	–38.4	–39.3
S_1/S_2 OCFs	33.6/33.6	34/34

Finally, to demonstrate experimentally the effectiveness of the proposed diagnosis method for the multiple switch faults, the results when OCF occurs in switches S_1 and S_2 are presented in Fig. 20, by taking the converter discharging mode as an example. The obtained results are similar to the simulation results in Fig. 5. It is seen that at the start, the converter works in a healthy state, and the residuals are near zero. Later, the OCF occurs in switch S_1, it is seen that the inductor current of the faulty module reduces to zero, and its residual e_1 increases to exceed the threshold to diagnose the fault. Applying the OCF to switch S_2, it is seen that the relevant residual e_2 would increase to strike the threshold, and the switch fault can be diagnosed. It can be concluded that the proposed method can diagnose multiple switch faults. This is because the residuals for each module are independent, as analyzed in Section III-C.

It is read from the oscilloscope that the diagnosis time for switch OCF is less than two switching periods, and the steady-state value of residual in the faulty module is summarized in Table III. It is clearly seen that these values agree with the calculated values by (17), (18), (19), and (20). The slight difference is mainly caused by the small deviation of the battery voltage from its nominal value during the experiments.

TABLE IV
COMPARISON OF SWITCH OPEN-CIRCUIT FAULT DIAGNOSIS APPROACHES

Ref.	Converter type	Diagnosis criterion	Switching frequency	Sampling time	Diagnosis time (Max.)	Robustness
Yahyaoui et al. [9]	Interleaved boost	Capacitor voltage	20 kHz	_ [1]	2.2ms	Medium
Nie et al. [13]	Boost	Inductor current slope sign	15 kHz	1 μs	$2T_s$ [2]	High
Pazouki et al. [17]	Interleaved boost	Input current evolution	{1,3,5} kHz	20 μs	$2T_s$	Medium to high
Ding [21]	Interleaved buck	Linear observer	25 kHz	_	$2T_s$ [3]	Medium to high
Badaoui et al. [26]	Buck/boost converter [4]	Global state observer	10 kHz	20 μs	$5T_s$	Medium to high
Proposed	Interleaved buck/boost [4]	Sliding mode observer	25 kHz	20 μs	$2T_s$	High

[1] Not specific; [2] Switching period; [3] Off-line validations; [4] Bidirectional converters.

VI. CONCLUSION

This article proposed a sliding mode observer-based robust switch fault diagnosis method for a bidirectional interleaved dc–dc buck/boost converter for the energy storage system. The sliding mode observer is designed to generate residuals for fault diagnosis using only the nominal converter model. It is demonstrated by simulation and experimental results that the proposed fault diagnosis method shows strong robustness to modeling imperfections and disturbances. The switch OCF can be diagnosed in less than two switching periods, which is comparable with the latest approaches, as given in Table IV. The proposed method has superiority in terms of sampling rate, implementation cost, and robustness against false alarms. The proposed method uses the inductor current as the diagnostic variable, which is already within the closed-loop control system. Therefore, it does not require additional sensors. The proposed method can be extended to other bidirectional power converters.

APPENDIX A

Define the positive definite function as $V = \frac{1}{2}\, \boldsymbol{e}^T \boldsymbol{e} > 0$, its derivative can be expressed as: $\dot{V} = \boldsymbol{e}^T\, \dot{\boldsymbol{e}}$. It follows from (5) and (8) that

$$\dot{V} = \boldsymbol{e}^T\, \boldsymbol{A}_0 \boldsymbol{e} - \boldsymbol{e}^T \boldsymbol{G} \mathrm{sgn}\left(\boldsymbol{e}\left(t\right)\right) - \boldsymbol{e}^T\left(t\right) \boldsymbol{f}_0\left(t\right). \tag{22}$$

Based on the known conditions $\boldsymbol{A}_0 < \boldsymbol{0}$ and $\boldsymbol{G} > \boldsymbol{0}$, one can obtain from (9) that

$$\dot{V} < -\boldsymbol{e}^T \boldsymbol{G} \mathrm{sgn}\left(\boldsymbol{e}\left(t\right)\right) - \boldsymbol{e}^T\left(t\right) \boldsymbol{f}_0\left(t\right). \tag{23}$$

Therefore, to ensure that $\dot{V} < 0$, the following condition must be satisfied:

$$\boldsymbol{e}^T \boldsymbol{G} \mathrm{sgn}\left(\boldsymbol{e}\left(t\right)\right) \geq \left|\boldsymbol{e}^T\left(t\right)\right| \left|\boldsymbol{f}_0\left(t\right)\right| \tag{24}$$

namely

$$g_k \geq \left|\boldsymbol{f}_0\left(k\right)\right|, k \;=\; 1, 2. \tag{25}$$

As there exist $V > 0$ and $\dot{V} < 0$, the stability of the sliding mode observer is thus proved.

APPENDIX B

The converter model can be expressed as

$$C\, \dot{x}_3 = \left(1 - d_1\right)\; x_1 + \left(1 - d_2\right) x_2 - x_3 / R \tag{26}$$

where x_3 is the output voltage, R is the load resistance.

Consider the positive-definite function [34]

$$V\left(x_1, x_2, x_3\right) \;= \frac{1}{2}\, L_1 x_1^2 + \frac{1}{2} L_2 x_2^2 + \frac{1}{2} C x_3^2 \tag{27}$$

which corresponds to the electrical energy stored in the converter system. It follows from (4) and (26) that the time derivative of (27) with trajectories is

$$\dot{V} = \; -r_1 x_1^2 - r_2 x_2^2 + x_1 v_b + x_2 v_b - x_3^2 / R. \tag{28}$$

Based on the Young's inequality and the bound $|v_b| \leq E$, one can derive from (28) that

$$\dot{V} \leq -\frac{r_1}{2} x_1^2 - \frac{r_2}{2} x_2^2 - x_3^2 / R + \frac{E^2}{2r_1} + \frac{E^2}{2r_2}. \tag{29}$$

It is noted that since $r_1 > 0$ and $r_2 > 0$, the last two terms of the right side of (29) are bounded. Therefore, all trajectories are bounded and converge to the set

$$\Omega = \left\{ \left(x_1, x_2, x_3\right) | \in \frac{r_1}{2} x_1^2 + \frac{r_2}{2} x_2^2 + x_3^2 / R < \frac{E^2}{2r_1} + \frac{E^2}{2r_2} \right\}. \tag{30}$$

REFERENCES

[1] A. Baroutaji, T. Wilberforce, M. Ramadan, and A. G. Olabi, "Comprehensive investigation on hydrogen and fuel cell technology in the aviation and aerospace sectors," *Renew. Sustain. Energy Rev.*, vol. 106, pp. 31–40, 2019.

[2] M. Obi and R. Bass, "Trends and challenges of grid-connected photovoltaic systems – A review," *Renew. Sustain. Energy Rev.*, vol. 58, pp. 1082–1094, 2016.

[3] F. Nadeem, S. M. S. Hussain, P. K. Tiwari, A. K. Goswami, and T. S. Ustun, "Comparative review of energy storage systems, their roles, and impacts on future power systems," *IEEE Access*, vol. 7, pp. 4555–4585, 2019.

[4] S. A. Gorji, H. G. Sahebi, M. Ektesabi, and A. B. Rad, "Topologies and control schemes of bidirectional dc–dc power converters: An overview," *IEEE Access*, vol. 7, pp. 117997–118019, 2019.

[5] S. Yang, A. Bryant, P. Mawby, D. Xiang, L. Ran, and P. Tavner, "An industry-based survey of reliability in power electronic converters," *IEEE Trans. Ind. Appl.*, vol. 47, no. 3, pp. 1441–1451, May/Jun. 2011.

[6] D. R. Espinoza-Trejo, L. M. Castro, E. Bárcenas, and J. P. Sánchez, "Data-driven switch fault diagnosis for dc/dc boost converters in photovoltaic applications," *IEEE Trans. Ind. Electron.*, vol. 71, no. 2, pp. 1631–1640, Feb. 2024.

[7] A. B. Rhouma, H. Meddeb, B. Gmati, S. K. El Khil, and C. Boccaletti, "Deep-learning based power switch fault diagnosis in dc/dc converters for photovoltaic applications," in *Proc. IEEE Int. Power Electron. Motion Control Conf.*, 2024, pp. 1–5.

[8] S. S. Khan and H. Wen, "A comprehensive review of fault diagnosis and tolerant control in DC-DC converters for DC microgrids," *IEEE Access*, vol. 9, pp. 80100–80127, 2021.

[9] R. Yahyaoui, A. De Bernardinis, A. Gaillard, and D. Hissel, "Switch short-circuit fault detection algorithm based on drain-to-source voltage monitoring for a fault-tolerant DC/DC converter," in *Proc. IEEE 42nd Annu. Conf. Ind. Electron. Soc.*, 2016, pp. 2212–2217.

[10] H. Givi, E. Farjah, and T. Ghanbari, "Switch and diode fault diagnosis in nonisolated DC-DC converters using diode voltage signature," *IEEE Trans. Ind. Electron.*, vol. 65, no. 2, pp. 1606–1615, Feb. 2018.

[11] Y. Huangfu, S. Zhuo, F. Chen, and S. Pang, "Evaluation and fault tolerant control of a floating interleaved boost converter for fuel cell systems," in *Proc. IEEE Ind. Appl. Soc. Annu. Meeting*, 2016, pp. 1–7.

[12] C. Li, Y. Yu, Z. Yang, W. Wang, and X. Peng, "A sensorless open-circuit fault identification method for interleaved boost converter," *IEEE Trans. Instrum. Meas.*, vol. 73, Jul. 2024, Art. no. 3525508.

[13] S. Nie, X. Pei, Y. Chen, and Y. Kang, "Fault diagnosis of PWM DC-DC converters based on magnetic component voltages equation," *IEEE Trans. Power Electron.*, vol. 29, no. 9, pp. 4978–4988, Sep. 2014.

[14] X. Pei, S. Nie, and Y. Kang, "Switch short-circuit fault diagnosis and remedial strategy for full-bridge DC-DC converters," *IEEE Trans. Power Electron.*, vol. 30, no. 2, pp. 996–1004, Feb. 2015.

[15] M. Shahbazi, E. Jamshidpour, P. Poure, S. Saadate, and M. R. Zolghadri, "Open- and short-circuit switch fault diagnosis for nonisolated DC-DC converters using field programmable gate array," *IEEE Trans. Ind. Electron.*, vol. 60, no. 9, pp. 4136–4146, Sep. 2013.

[16] E. Jamshidpour, P. Poure, and S. Saadate, "Photovoltaic systems reliability improvement by real-time FPGA-based switch failure diagnosis and fault-tolerant DC-DC converter," *IEEE Trans. Ind. Electron.*, vol. 62, no. 11, pp. 7247–7255, Nov. 2015.

[17] E. Pazouki, Y. Sozer, and J. A. De Abreu-Garcia, "Fault diagnosis and fault-tolerant control operation of nonisolated DC-DC converters," *IEEE Trans. Ind. Appl.*, vol. 54, no. 1, pp. 310–320, Jan./Feb. 2018.

[18] E. Ribeiro, A. J. M. Cardoso, and C. Boccaletti, "Open-circuit fault diagnosis in interleaved DC-DC converters," *IEEE Trans. Power Electron.*, vol. 29, no. 6, pp. 3091–3102, Jun. 2014.

[19] F. Bento and A. J. M. Cardoso, "Open-circuit fault diagnosis and fault tolerant operation of interleaved DC-DC boost converters for homes and offices," *IEEE Trans. Ind. Appl.*, vol. 55, no. 5, pp. 4855–4864, Sep./Oct. 2019.

[20] M. W. Ahmad, N. B. Y. Gorla, H. Malik, and S. K. Panda, "A fault diagnosis and postfault reconfiguration scheme for interleaved boost converter in PV-based system," *IEEE Trans. Power Electron.*, vol. 36, no. 4, pp. 3769–3780, Apr. 2021.

[21] S. Ding, *Model-Based Fault Diagnosis Techniques: Design Schemes, Algorithms and Tools*. Berlin, Germany: Springer, 2008.

[22] J. Poon, P. Jain, I. C. Konstantakopoulos, C. Spanos, S. K. Panda, and S. R. Sander, "Model-based fault detection and identification for switching power converters," *IEEE Trans. Power Electron.*, vol. 32, no. 2, pp. 1419–1430, Feb. 2017.

[23] N. Wassinger, E. Penovi, R. G. Retegui, and S. Maestri, "Open-circuit fault identification method for interleaved converters based on time domain analysis of the state observer residual," *IEEE Trans. Power Electron.*, vol. 34, no. 4, pp. 3740–3749, Apr. 2019.

[24] L. Xu, R. Ma, R. Xie, J. Xu, Y. Huangfu, and F. Gao, "Open-circuit switch fault diagnosis and fault-tolerant control for output-series interleaved boost DC-DC converter," *IEEE Trans. Transp. Electrific.*, vol. 7, no. 4, pp. 2054–2066, Dec. 2021.

[25] S. Zhuo, A. Gaillard, L. Xu, C. Liu, D. Paire, and F. Gao, "An observer-based switch open-circuit fault diagnosis of DC-DC converter for fuel cell application," *IEEE Trans. Ind. Appl.*, vol. 56, no. 3, pp. 3159–3167, May/Jun. 2020.

[26] Y. Badaoui, A. A. Djamel, A. Gouichiche, A. Safa, and A. Chibani, "A linear observer design for fast open switch fault detection of interleaved boost converters," in *Proc. 2nd IEEE Ind. Electron. Soc. Annu. -Line Conf.*, 2023, pp. 1–6.

[27] S. Ding, D. Tang, J. Hang, J. Zhao, and S. Gui, "Robust open-switch fault diagnosis of bidirectional DC/DC converters based on extended Kalman filter with multiple corrections," *IEEE Trans. Circuits Syst. I, Reg. Papers*, vol. 71, no. 9, pp. 4363–4374, Sep. 2024.

[28] J. Hang, C. Ge, S. Ding, W. Li, Y. Huang, and W. Hua, "A global state observer-based open-switch fault diagnosis for bidirectional DC-DC converters in hybrid energy source system," *IEEE Trans. Power Electron.*, vol. 38, no. 10, pp. 13085–13098, Oct. 2023.

[29] A. Levant, "Principles of 2-sliding mode design," *Automatica*, vol. 43, pp. 576–586, 2007.

[30] P. Luo, Z. Yin, Z. Zhang, Y. Zhang, P. Zhang, and J. Liu, "Diversified diagnosis strategy for PMSM inter-turn short-circuit fault via novel sliding mode observer," *IEEE Trans. Power Electron.*, vol. 39, no. 4, pp. 4149–4159, Apr. 2024.

[31] S. Xu et al., "Multiple open-switch fault diagnosis for three-phase four-leg inverter under unbalanced loads via interval sliding mode observer," *IEEE Trans. Power Electron.*, vol. 39, no. 6, pp. 7607–7619, Jun. 2024.

[32] S. Xu, X. Chen, W. Yang, F. Liu, and Y. Chai, "Current sensor incipient fault diagnosis in PMSM drive systems using novel interval sliding mode observer," *IEEE Trans. Instrum. Meas.*, vol. 73, Jan. 2024, Art. no. 3508211.

[33] S. Zhuo, S. Jin, X. Liu, H. Bai, Y. Huangfu, and F. Gao, "Robust voltage control with resonant extended state observer for hybrid fuel cell system," *IEEE Trans. Power Electron.*, vol. 39, no. 5, pp. 5462–5472, May 2024.

[34] A. Astolfi, D. Karagiannis, and R. Ortega, *Nonlinear and Adaptive Control With Applications*. Berlin, Germany: Springer, 2008.